Vortex Induced Vibration of Rotating Spheres

M. M. Rajamuni, M. C. Thompson and K.Hourigan

Department of Mechanical and Aerospace Engineering
Monash University, Clayton, Victoria 3168, Australia

Abstract

The Vortex Induced Vibration (VIV) of an elastically mounted transversely rotating sphere is studied numerically. The sphere is constrained to oscillate orthogonal to the plane made by the direction of the freestream and the axis of sphere rotation. The sphere motion was modelled by a spring-mass system, while the flow was modelled using the incompressible Navier-Stokes equations. The coupled fluid-structure system was solved with the finite-volume based CFD package OpenFOAM by using a newly developed solver. Here, the Navier-Stokes equations were solved in a non-inertial frame centred on the sphere. The effect of the sphere rotation on the VIV was studied at Reynolds number, $Re = 300$, the density ratio between solid and fluid was $m^* = 3.8197$, and the non-dimensional rotation rate, α, was varied between 0 and 1.5. In addition, the reduced velocity, U^*, was varied between 3.5 and 11 to investigate the oscillation amplitude response. Without rotation, the sphere oscillation was found to be synchronised with the vortex shedding frequency, with maximum oscillation amplitude of approximately 0.4 diameters. Two hairpin type vortex streets were observed in the synchronisation regime. With the symmetry breaking introduced by the forced rotation, the oscillation amplitude decreased and the synchronisation regime was narrowed. Furthermore, VIV was suppressed completely for $\alpha > 1$.

Introduction

Fluid-Structure Interaction (FSI) has been an important research topic in fluid dynamics for many years. When a fluid flows past a solid structure, a large-amplitude fluctuating pressure force can be created near the solid body due to the formation and subsequent shedding of vortices into the wake. These vortices can induce structural vibration (in this case *Vortex Induced Vibration* or VIV), which may increase the fatigue damage or sometimes even the failure of structures. A large number of experimental and numerical studies have been undertaken to understand the fundamentals of VIV (for a summary see [8, 10, 12]). Cylindrical structures were used mostly in those studies, despite the fact that there are numerous applications involving other body shapes including spherical bodies.

Recently, the nature of VIV of a sphere began to be revealed once Williamson [11] experimentally found that the sphere oscillates remarkably at a transverse saturation amplitude of close to two diameters peak to peak. He recognised that plotting the amplitude response versus reduced velocity ($U^* = U/f_nD$, where U is the free stream velocity, f_n is the natural frequency of the system, and D is the sphere diameter), was more suitable for interpreting and classifying the behaviour than using the amplitude response versus the Reynolds number. He observed that there were two different modes of oscillation, namely mode I and mode II. These two modes appeared within the velocity regime $U^* \sim 5$–10, and the body oscillation frequency, f, was close to the static body vortex shedding frequency, f_{vo} ($f_{vo}/f \sim 1$), which clearly indicates that these vibrations are induced from the vortex shedding behind the sphere. In addition to these two modes of vibration, Jauvtis et al. [3] observed another mode of vibration (mode III), which appeared within

the reduced velocity range $U^* \sim 20$–40. Aside from these experimental studies, a few numerical studies have examined the VIV of a sphere at low Reynolds numbers [1, 9].

The influence of rotation on the motion of a sphere has been studied for centuries. Early research studies carried out by Benjamin Robinson in 1742 observed that a sphere experiences a transverse force ('Magnus force') when it propagates with a transverse rotation. Heinrich Gustav Magnus demonstrated that the rotational motion of the sphere is responsible for this transverse force. Later, researchers found that the magnitude of this force increases with the rotation rate, α ($= \omega D/2U$, where ω is the sphere angular velocity). In more recent studies, Giacobello et al. [2] and Kim [5] investigated the effects of transverse rotation on the wake behind a sphere and on the forces exerted on the sphere at $Re = 100, 250, 300$, for $\alpha \leq 1.2$. They found that at $Re = 100$, the axisymmetric flow that appeared for no rotation became planar symmetric with a double-threaded wake in the presence of rotation. At $Re = 250$ and 300, the flow underwent a series of different transitions between steadiness and unsteadiness as the rotation rate was increased. Their studies also revealed that the drag coefficient, $C_d = F_d/(0.5\rho U\pi(D/2)^2)$, and the lift coefficient, $C_l = F_l/(0.5\rho U\pi(D/2)^2)$, increased with the rotation rate for all three Reynolds numbers considered, where F_d is the drag force, F_l is the lift force, and ρ is the density of the fluid.

Despite the fact that rotation greatly influences the motion of a sphere, to the authors' knowledge, no experimental or numerical studies have reported on the flow-induced vibration of a rotating sphere. Therefore, in the present work, effects of transverse rotation on the vortex induced vibration of a sphere are investigated by examining the sphere displacement, forces exerted on the sphere and wake structures behind the sphere at $Re = 300$ for rotation rate, α, = 0–1.5, and reduced velocity, U^*, = 3.5–11. The structure of this paper is organised as follows: the next section describes the numerical methods used together with validation studies; the sphere response to VIV and wake structures are presented in the results section, followed by a conclusion.

Numerical Methods

Problem Set-up

A uniform flow (in the x direction with magnitude U) past a transversely rotating (axis of rotation $= -z$, angular velocity $= \omega$), elastically mounted (free to translate on y axis) sphere of diameter D was studied numerically using the CFD package, OpenFOAM. A cubic domain with a side length of $100D$ was chosen for the computational domain with the sphere at its centre (see figure 1).

A non-deformable mesh was chosen for the fluid domain to improve the efficiency of solving the couple fluid-solid system. Fluid flow was modelled in a reference frame attached to the centre of the sphere. The motion of the reference frame was taken into the account by updating the velocity boundary conditions at all outer boundaries except the outlet at each time step.

The boundary conditions were chosen as shown in figure 1. At the sphere surface, no slip and no penetration boundary conditions were applied together with a rotating wall velocity.
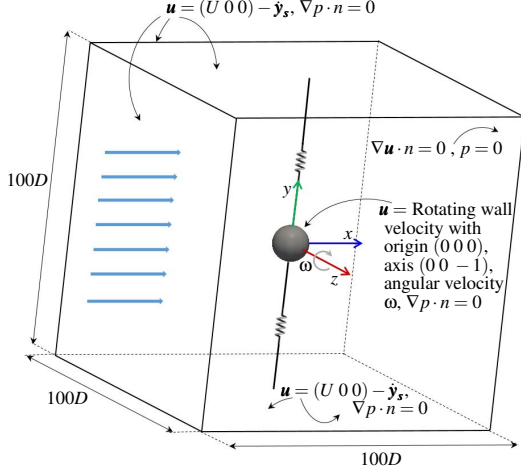

Figure 1: Schematic of the computational domain and boundary conditions: $\boldsymbol{u}$ - fluid velocity vector, p - fluid pressure, n - outward unit normal vector, D - sphere diameter, $\dot{\boldsymbol{y}}_s$ - sphere velocity vector, ω sphere angular velocity.

Governing Equations

The reference frame of the fluid is non-inertial since it accelerates according to the sphere motion. Thus, the momentum equation needs to be adjusted accordingly. This can be done by adding the acceleration of the sphere to the momentum equation on the right, acting as a fictitious force in the opposite direction. The sphere motion was assumed to behave as a spring-mass system and the fluid was assumed incompressible and viscous. The coupled fluid-solid system can be described by the Navier-Stokes equations, given in equations (1) and (2), together with the equation governing the motion of the sphere in equation (3).

$$\frac{\partial \mathbf{u}}{\partial t} = -(\mathbf{u}\cdot\nabla)\mathbf{u} - \nabla p + \nabla\cdot\nu\nabla\mathbf{u} - \ddot{\boldsymbol{y}}_s, \qquad (1)$$

$$\nabla\cdot\mathbf{u} = 0 \qquad (2)$$

$$m\,\ddot{\boldsymbol{y}}_s + k\,\boldsymbol{y}_s = \mathbf{f}_l \qquad (3)$$

Here, $\mathbf{u} = \mathbf{u}(x,y,z,t)$ is the velocity vector field, p is the scalar pressure field, ν is the kinematic viscosity, $\boldsymbol{y}_s$ is the sphere displacement vector, $\ddot{\boldsymbol{y}}_s$ is the sphere acceleration vector, m is the mass of the sphere, k is the structural spring constant, and $\mathbf{f}_l$ is the flow-induced force vector on the sphere due to pressure and viscous shear forces. Note that $\boldsymbol{y}_s$, $\ddot{\boldsymbol{y}}_s$, and $\mathbf{f}_l$ are vectors with zero x and z components (since the sphere motion was restricted to the y direction).

A new solver (namely vivicoFoam) was developed, based on the 'icoFoam' solver for laminar flows, to solve the coupled system defined by the above equations. This solver is employed with a predictor-corrector method that iterates until the fluid force and solid acceleration converge within given error bounds.

Validation Studies

The flow past a stationary and transversely rotating sphere were studied using the 'icoFoam' solver at $Re = 300$ and rotation rates, $\alpha = 0$, 0.5 and 1. Calculated values for the time-averaged drag coefficient, $\bar{C}_d$, time-averaged lift coefficient, $\bar{C}_l$, and Strouhal number, St, are compared with other studies in

Study	α	$\bar{C}_d$	$\bar{C}_l$	St
Present	0	0.665	0.070	0.137
Kim et al. [6]	0	0.657	0.067	0.137
Johnson and Patel [4]	0	0.656	0.069	0.137
Present	0.5	0.820	0.473	-
Giacobello et al. [2]	0.5	0.867	0.472	-
Present	1	0.958	0.615	0.421
Kim [5]	1	0.940	0.600	0.421
Giacobello et al. [2]	1	0.921	0.607	0.428

Table 1: Comparison of computed time-averaged drag coefficient, $\bar{C}_d$, time-averaged lift coefficient, $\bar{C}_l$, and Strouhal number, St, at $Re = 300$ and $\alpha = 0$, 0.5, and 1 with other numerical studies.

table 1. For both the stationary sphere and the transversely rotating sphere, the present results are in good agreement with the reported literature [4, 6, 2, 5].

To validate the numerical code (vivicoFoam solver) developed for the VIV simulations, a series of simulations were conducted with parameters chosen from [7]. The mass ratio was set to $m^* = 10$ and damping ratio to $\zeta = 0.01$ (in this case, the cylinder displacement was modelled by a spring-mass-damper system). The Reynolds number is $Re = 200$ and the reduced velocity range is from $U^* = 3$ to 7.5. Figure 2 compares our results for maximum oscillation amplitude, A'_{max}; peak lift coefficient, $C'_{l,max}$; frequency of the oscillation $f^* = f/f_n$; and average phase angle between lift force and cylinder displacement, ϕ, with results from Leontini et al. [7]: the results we obtained are almost identical, with minor differences probably due to the slightly different blockage ratios. This study provides validation for the new solver.

Results

A series of simulations were conducted on flow past an elastically mounted (on the y axis), transversely rotating (in the $-z$ direction) sphere at Reynolds number $Re = 300$, mass ratio $m^* = 3.8197$, rotation rates $\alpha = 0$–1.5, and reduced velocities $U^* = 3.5$–11. The Reynolds number of the flow was prescribed through the kinematic viscosity in equation (1) ($\nu = DU/Re$) and the reduced velocity was prescribed through the spring constant in the solid motion equation ($k = 4m\pi^2/U^{*2}$).

Sphere Response

The non-dimensional sphere displacement, A, is defined to be the y component of the solid displacement vector normalised by the sphere diameter ($A = \boldsymbol{y}_s \cdot (0\ 1\ 0)/D$). The sphere response curves in terms of A are shown in figure 3: (a) time averaged sphere displacement, $\bar{A}$; (b) maximum oscillation amplitude, A'_{max}; (c) frequency of oscillation, $f^* = f/f_n$; at $Re = 300$, $m^* = 3.1897$, for the reduced velocity range $U^* = 3.5$–11 at each of the rotation rates considered. As can be seen from figure 3 (a), the mean displacement, $\bar{A}$, was increased with the rotation rate up to $\alpha = 1$ due to Magnus force, and this was more prominent as the reduced velocity increased. However, as α increased from 1 to 1.5, $\bar{A}$ did not increase further, instead it slightly decreased. At $\alpha = 0$, $\bar{A}$ was zero at the reduced velocity range $U^* = 5.5$–10, as expected. Figure 3 (b) shows that at those U^* values and $\alpha = 0$, the sphere oscillated greatly with maximum oscillation amplitude of approximately $0.4D$. Furthermore, the sphere oscillation frequency was synchronised with
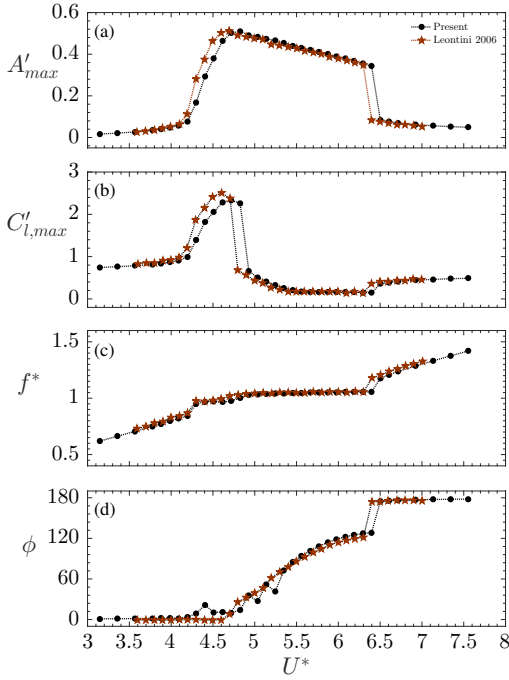
Figure 2: Response of an elastically mounted cylinder as a function of reduced velocity: $Re = 200$, $m^* = 10$, $\zeta = 0.01$. (a) maximum oscillation amplitude, A'_{max}; (b) peak lift coefficient, $C'_{l,max}$; (c) frequency of the oscillation $f^* = f/f_n$; (d) average phase angle between lift force and cylinder displacement.

the system's natural frequency (figure 3 (c)), which indicates this is a Vortex Induced Vibration response. Interestingly, when the sphere had imposed on it a forced rotation, the maximum oscillation amplitude decreased with α and it was completely suppressed at $\alpha = 1.5$. Moreover, the synchronization regime narrowed with increasing α. Vortex shedding frequencies at $\alpha = 0.2$, 0.5 and 1 were also synchronized with the natural frequency, as can be seen from figure 3 (c)). Therefore, sphere oscillations at those rotation rates are clearly due to VIV.

Force Measurements

The variation of the time-averaged drag coefficient, $\bar{C}_d$, and the lift coefficient, $\bar{C}_l$, with U^* at each α considered are given in figures 4 (a) and (b), respectively. The dashed lines in figure 4 refer to $\bar{C}_d$ and $\bar{C}_l$ calculated with flow past a rigidly mounted and transversely rotating sphere at each α. For rigidly mounted sphere cases, $\bar{C}_d$ increased with α for all values in the range while $\bar{C}_l$ increased up to $\alpha = 1$ and then decreased slightly. The pattern of variation of $\bar{C}_l$ with α is consistent with the pattern of variation of $\bar{A}$ with α. For elastically mounted sphere cases, in the synchronisation regime, $\bar{C}_d$ increased from the nominal value, with the increments reducing with increasing α (figure 4 (a)). A similar trend can be seen in $\bar{C}_l$ as well, where $\bar{C}_l$ decreased in the synchronisation regime from the nominal value, again with the decrements reducing with increasing α (figure 4 (b)). At $\alpha = 1.5$, neither $\bar{C}_d$ nor $\bar{C}_l$ varied from the nominal value. This is presumably due to the suppression of vortex shedding at this rotation rate.

Wake Structures

Figure 5 shows the wakes structures in the synchronisation regime (at $U^* = 6$) at each rotation rate considered. At $\alpha = 0$, two streets of hairpin-type vortex loops were observed. This
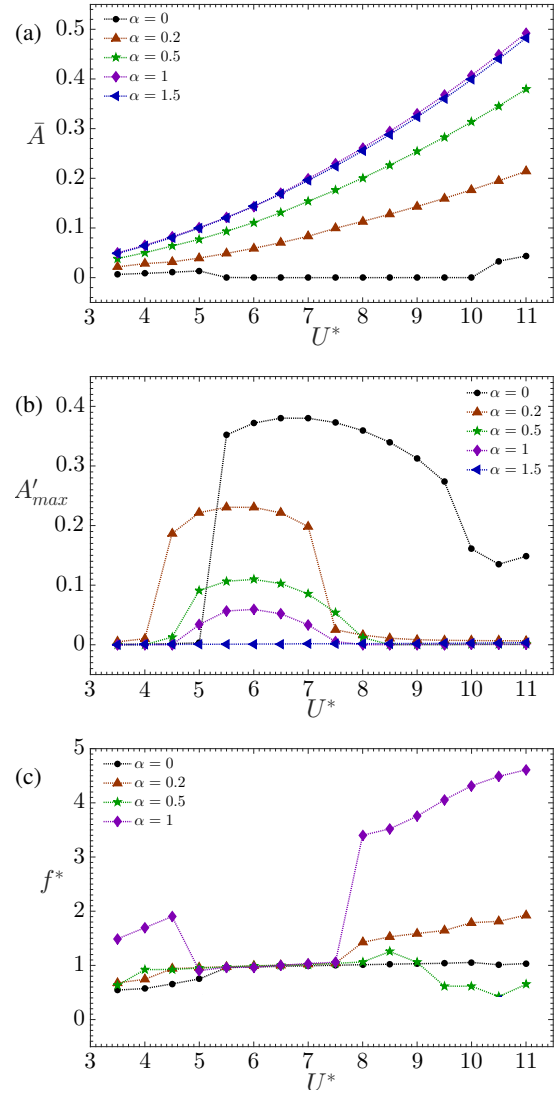

Figure 3: Response of an elastically mounted (on y axis) rotating (on $-z$ direction) sphere as a function of reduced velocity at the rotation rates $\alpha = 0$, 0.2, 0.5, 1, and 1.5: $Re = 300$, $m^* = 3.1897$, (a) time-averaged non-dimensional sphere displacement, $\bar{A}$; (b) maximum oscillation amplitude, A'_{max}; (c) oscillation frequency normalised by the system natural frequency, $f^* = f/f_n$.

wake structure is identical to the hairpin type wake observed by Behara [1] on VIV of a sphere with $3DOF$ at $Re = 300$.

As α increased from 0, the wake was deflected downward ($-y$ direction) due to Magnus effect. In addition, this deflection was more prominent as α increased. The equal strength vortex streets observed at $\alpha = 0$ became uneven with the sphere rotation. The lower vortex street became stronger than the upper vortex street with increasing α (see figure 5). This unevenness of the strength of the vortex streets is responsible for the decrease of the amplitude response with α. At $\alpha = 1$, the upper vortex street is obscured and the vortex loops on the lower street near the sphere strongly resemble the vortex structures observed by Giacobello [2] and Kim [5] in their studies of the flow past a transversely rotating sphere at $Re = 300$ and $\alpha = 1$. At $\alpha = 1.5$, a double threaded steady wake was observed at each U^*. This shows clear evidence for VIV suppression.
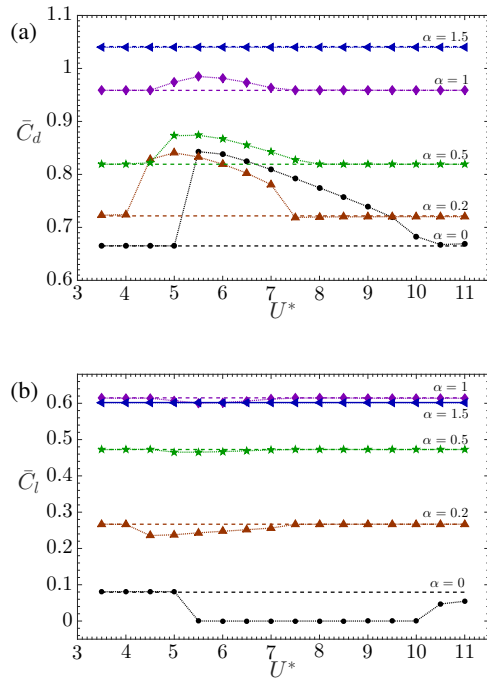
Figure 4: Time-averaged (a) drag coefficient, $\bar{C}_d$; (b) lift coefficient, as a function of reduced velocity, U^* for $\alpha = 0$, 0.2, 0.5, 1, and 1.5. Dashed lines represent the values of $\bar{C}_d$ and $\bar{C}_l$ calculated with a rigidly mounted sphere at each α.
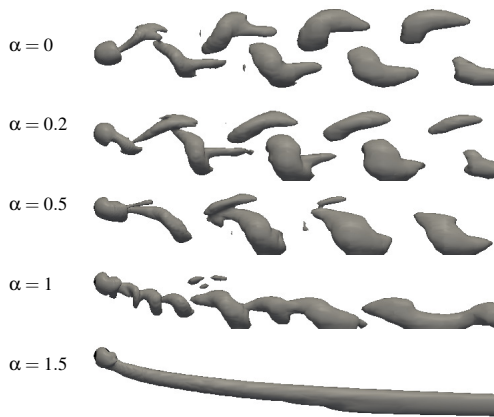

Figure 5: Instantaneous vortical structures (Iso-surfaces of $Q = 0.001$ in x-y plane) of vortex induced vibration of a transversely rotating sphere at $Re = 300$, $m^* = 3.8197$, $U^* = 6$, for $\alpha = 0$, 0.2, 0.5, 1, and 1.5.

Conclusions

The effect of transverse rotation on the vortex induced vibration of a sphere was studied at Reynolds number $Re = 300$, mass ratio $m^* = 3.8197$, for rotation rates 0–1.5. For no rotation, the sphere oscillated with a maximum oscillation amplitude of approximately $0.4D$ by synchronising with its natural frequency in the reduced velocity regime $U^* = 5.5$–11. As the rotation rate increased from 0, the oscillation amplitude decreased and the synchronisation regime narrowed. Once the rotation rate reached 1.5, the oscillation was completely suppressed. Two antisymmetric hairpin-type vortex trails were shed behind the sphere under no rotation. As the wake deflected into the downward direction (-y direction) under imposed rotation, the vortex loops become stronger in the lower trail than the vortex loops in the upper trail. This symmetry breaking is responsible for

the decrease in amplitude response and the narrowing of the synchronisation regime. With these observations, we can conclude that VIV persists at small rotation rates, but that the alternation/suppression of vortex shedding caused by the Magnus effect as the rotation rate is increased, does in fact lead to suppression of VIV at higher rotation rates, in spite of the freedom of the sphere to oscillate.

References

[1] Behara, S., Borazjani, I. and Sotiropoulos, F., Vortex-induced vibrations of an elastically mounted sphere with three degrees of freedom at Re = 300: hysteresis and vortex shedding modes, *Journal of Fluid Mechanics*, **686**, 2011, 426–450.

[2] Giacobello, M., Ooi, A. and Balachandar, S., Wake structure of a transversely rotating sphere at moderate Reynolds numbers, *Journal of Fluid Mechanics*, **621**, 2009, 103–130.

[3] Jauvtis, N., Govardhan, R. and Williamson, C., Multiple modes of vortex-induced vibration of a sphere, *Journal of Fluids and Structures*, **15**, 2001, 555–563.

[4] Johnson, T. and Patel, V., Flow past a sphere up to a Reynolds number of 300, *Journal of Fluid Mechanics*, **378**, 1999, 19–70.

[5] Kim, D., Laminar flow past a sphere rotating in the transverse direction, *Journal of mechanical science and technology*, **23**, 2009, 578–589.

[6] Kim, J., Kim, D. and Choi, H., An immersed-boundary finite-volume method for simulations of flow in complex geometries, *Journal of Computational Physics*, **171**, 2001, 132–150.

[7] Leontini, J., Thompson, M. and Hourigan, K., The beginning of branching behaviour of vortex-induced vibration during two-dimensional flow, *Journal of Fluids and Structures*, **22**, 2006, 857–864.

[8] Parkinson, G., Phenomena and modelling of flow-induced vibrations of bluff bodies, *Progress in Aerospace Sciences*, **26**, 1989, 169 – 224.

[9] Peter, S. and De, A., Wake instability modes for forced transverse oscillation of a sphere, *Ocean Engineering*, **115**, 2016, 48 – 59.

[10] Sarpkaya, T., A critical review of the intrinsic nature of vortex-induced vibrations, *Journal of Fluids and Structures*, **19**, 2004, 389–447.

[11] Williamson, C. and Govardhan, R., Dynamics and forcing of a tethered sphere in a fluid flow, *Journal of Fluids and Structures*, **11**, 1997, 293 – 305.

[12] Williamson, C. and Govardhan, R., Vortex-induced vibrations, *Annu. Rev. Fluid Mech.*, **36**, 2004, 413–455.